Influence of Microscopic Strain Heterogeneity on the Formability of Martensitic Stainless Steel

Alvise Miotti Bettanini[1, a)], Laurent Delannay[1, b)], Pascal J. Jacques[1, c)], Thomas Pardoen[1, d)], Guillaume Badinier[2, e)], Jean-Denis Mithieux[2, f)]

[1] *Institute of Mechanics, Materials and Civil Engineering, Université catholique de Louvain, B-1348 Louvain-la-Neuve, Belgium*
[2]*Aperam Research Center, BP 15, 62230 Isbergues, France*

[a)] Corresponding author: alvise.miotti@uclouvain.be
[b)] laurent.delannay@uclouvain.be
[c)] pascal.jacques@uclouvain.be
[d)] thomas.pardoen@uclouvain.be
[e)] guillaume.badinier@aperam.com
[f)] jeandenis.mithieux@aperam.com

Abstract. Both finite element modeling and mean field (Mori-Tanaka) modeling are used to predict the strain partitioning in the martensite-ferrite microstructure of an AISI 410 martensitic stainless steel. Numerical predictions reproduce experimental trends according to which macroscopic strength is increased when the dissolution of carbides leads to carbon enrichment of martensite. However, the increased strength contrast of ferrite and martensite favours strain localization and high stress triaxiality in ferrite, which in turn promotes ductile damage development.

INTRODUCTION

Martensitic stainless steels (MSS) show a good combination of properties such as strength, ductility, fatigue and oxidation resistance, while being a cost-effective solution due to the absence of expensive nickel in the chemical composition and high quenching ability, that makes MSS virtually insensitive to the cooling rate [1]. All these characteristics make MSS an attractive materials choice for automotive applications.

MSS are Fe-Cr-C alloy with a minimum amount of 12wt% Cr and C in the range of 0.1 to 1wt%. Thus, depending on the composition and processing history, the room temperature equilibrium of these steels consists of a large volume fraction of martensite, residual ferrite and dispersions of carbides with different stoichiometry and size [2], [3]. By far the most common MSS is the 12wt% Cr, 0.1wt% C AISI 410 stainless steel, which, after standard industrial processing, presents a structure of ~80vol% martensite and ~20vol% ferrite. In addition, undissolved chromium carbides are often found in the ferritic phase after heat treatments.

Unfortunately, the mechanical strength contrast between ferrite and martensite causes strain heterogeneity at the microstructure level as recently reported in dual-phase steels by Tasan et al. [4] and documented in the literature with µ-DIC measurements [5], [6], [7]. Pierman et al. [8] studied the plastic behaviour of DP steels by systematically varying the martensite volume fraction, martensite carbon content and phase morphology. They found that the ductility decreases with increasing martensite carbon content in structures with large martensite volume fraction (60 vol%). Likewise, Taylor et al. [9] and Hudgins et al. [10] found a negative trend between local formability and phase strength ratio in a DP980 steel, which is also confirmed by a recent study on the ductility of a Nb-modified martensite-ferrite stainless steel [21]. These results indicate that larger strength heterogeneities cause strain localisation in dual phase steels. As a consequence, this could promote damage nucleation at critical microstructural features like precipitates or grain boundaries [11], [12], [13], [14].

To better understand the contribution of strain partitioning on the onset of damage initiation in dual phase materials, micromechanical modelling can be used. Kumar et al. [15] produced statistically equivalent dual phase microstructure and qualitatively studied the effect of phase distribution on the strain heterogeneity with finite element methods. More recently, de Geus et al. [16,17] took a similar approach to study the effect of phase mechanical contrast and space arrangement on strain partitioning. They found that strain partitioning in the soft phase increased with mechanical contrast and the confinement of the soft phase. In the present work, a combined experimental numerical approach has been followed to investigate the strain heterogeneities in MSS in order_to understand the impact on ductility.

EXPERIMENTAL OBSERVATIONS

The as-received material was heat treated with three different austenization conditions to produce a constant ferrite/martensite ratio of approximately 80vol% martensite and 20vol% ferrite, while dissolving the carbides originally present in the structure. This procedure increased the martensite carbon content and hence the strength of martensite while leaving the ferrite phase unchanged. The local hardness of the three microstructures was then measured with nanoindentation by probing an area of 45 µm x 20 µm with an average distance between indents of 2.5 µm. A total of 200 indents for each microstructure were then analysed. Table 1 shows the average hardness values in ferrite and martensite for the three microstructures, it was observed that average hardness of martensite increased with the heat treatment temperature, while the ferrite hardness was not largely affected by the processing conditions. FIGURE 1 shows the hardness map measured in the microstructure heat-treated at 975°C for 5 minutes. The hardness contrast between the soft ferrite (blue) and the hard martensite (red) regions is visible in the image. Interestingly, the largest hardness values appear in the martensite regions encircled by multiple ferrite grains.

Next, the mechanical properties of the three microstructures were measured using uniaxial tension and bending tests. It was observed that the true fracture strain decrease with increasing processing temperature, as shown in figure 2a. Later, the same trend was found during the V-bending tests (figure 2b), which show that the energy absorbed by the material before crack initiation (black triangles in figure 2b), decrease for microstructures with higher average martensite hardness. Hence, both tests indicated a reduction of the ductility with an increase of the martensite hardness and of the mechanical strength contrast in the microstructures.

TABLE 1. Average nanohardness (GPa) measurements in ferrite and martensite for the three heat treatments. Martensite hardness increases as temperature rises. Conversely, ferrite hardness is insensitive to the heat treatment. Thus, hardness contrast between the two phases increases with increasing austenization temperature.

Austenization Temperature (°C)	Ferrite Hardness (GPa)	Martensite Hardness (GPa)
875	2.29	3.36
900	2.30	3.46
975	2.34	3.61

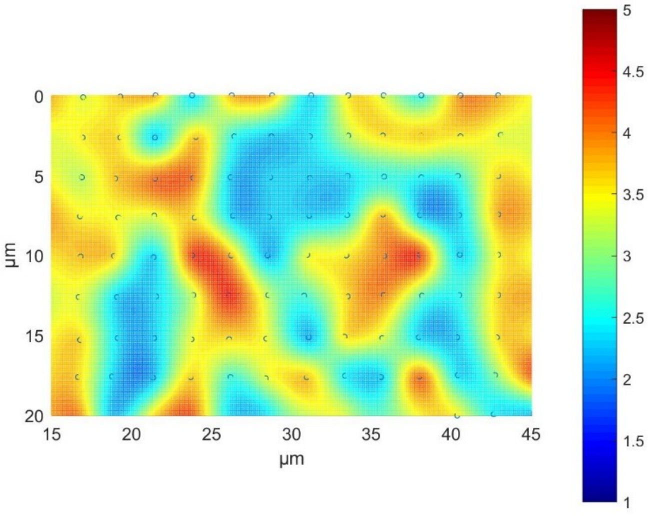

FIGURE 1. Detailed view of the hardness interpolation map produced in MATLAB for the microstructure heat treated at 975°C. The blue regions represent the soft ferrite islands, while the red regions are hard martensite. Peaks in hardness seem to occur when martensite is confined by soft ferrite regions, which contain the main carbon sources (chromium carbides).

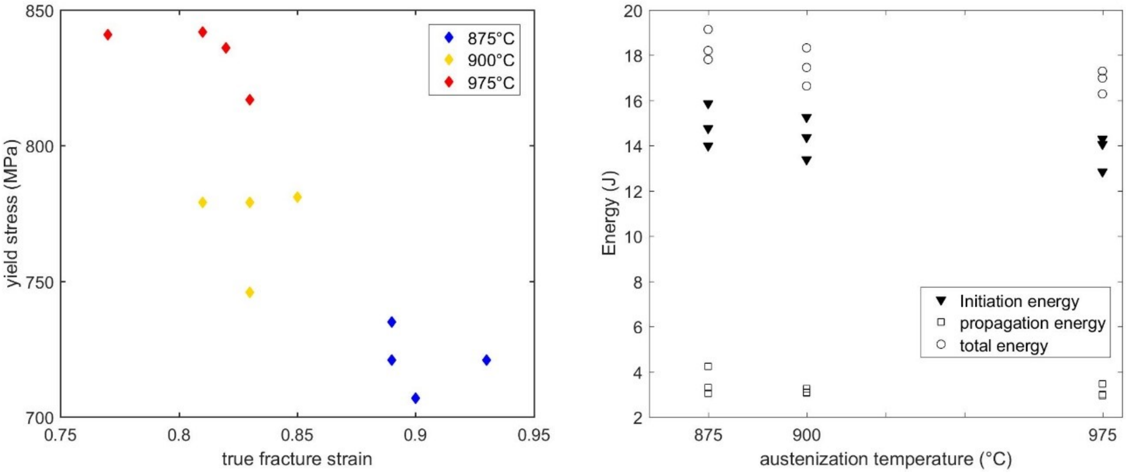

(a) (b)

FIGURE 2. Summary of the mechanical results. a) shows the yield stress and the fracture strain values for the three heat treatments and b) shows the energy absorbed by the material during the bending test. Both tensile and bending tests indicate a decrease in ductility for microstructure heat treated at higher temperature.

MODELING OF THE MICROSCOPIC STRAIN FIELD

After heat treatment, the microstructure consists of ~20vol% of ferrite inclusions in a continuous martensite matrix. Microstructural observations have also shown that ductile damage initiates inside ferrite.

The mechanical response has first been predicted using a mean field model relying on Eshelby's solution of the isolated inclusion inside a homogeneous elastic medium. Spherical ferrite inclusions were considered and the isotropic elastic-plastic responses of the two phases were linearized using a secant approach [18].

Then simulations were performed using a finite element model containing 108 ferrite grains shaped as truncated octahedrons [19]. The ferrite grains were distributed randomly inside a 3D periodic microstructure (Fig. 3) while preserving a minimum distance of one tenth of the grain diameter between two adjacent ferrite grains. Such martensite ligaments were observed experimentally. They ensure that the simulated ferrite grains are inclusions of identical size. Two types of microstructures were considered. In the *clustered* microstructure, each ferrite grain is adjacent to at least two other ferrite grains. In the *unclustered* microstructure, each ferrite grain is adjacent to at most two other ferrite grains.

The strain hardening of individual phases was reproduced using the following law:

$$\sigma_y = \sigma_{sat} - (\sigma_{sat} - \sigma_{y0}) \exp(-h_1 * p) + h_2 * p \tag{1}$$

where p is the accumulated equivalent plastic strain, σ_{y0} is the initial yield stress and h_1, h_2 and σ_{sat} are hardening parameters. The fitted parameter values are listed in Table 2.

TABLE 2. List of parameters used to reproduce the hardening behavior of phases as described in equation 1. Ferrite flow behavior is not affected by the heat treatments.

Phase	σ_{y0}	σ_{sat}	h_1	h_2
Ferrite	320	620	15	0
Martensite, 875°C	915	1065	35	55
Martensite, 900°C	1115	1265	20	50

Martensite, 975°C	1230	1350	15	50

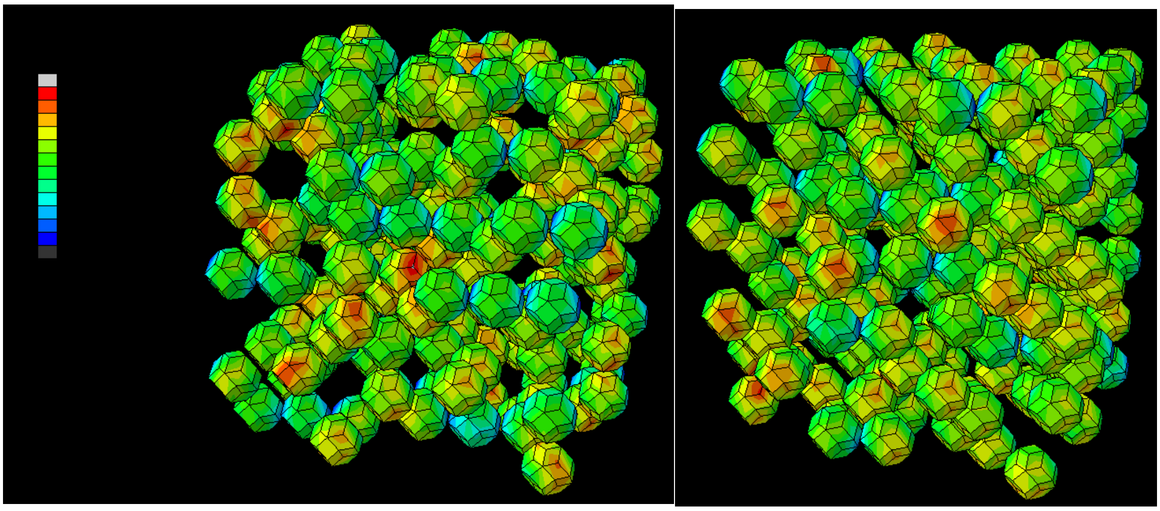

FIGURE 3. Periodic microstructure modelled using finite elements. Only the ferrite grains are shown. They are coloured according to the equivalent plastic strain at the early steps of deformation in the clustered (left) and the unclustered (right) microstructures.

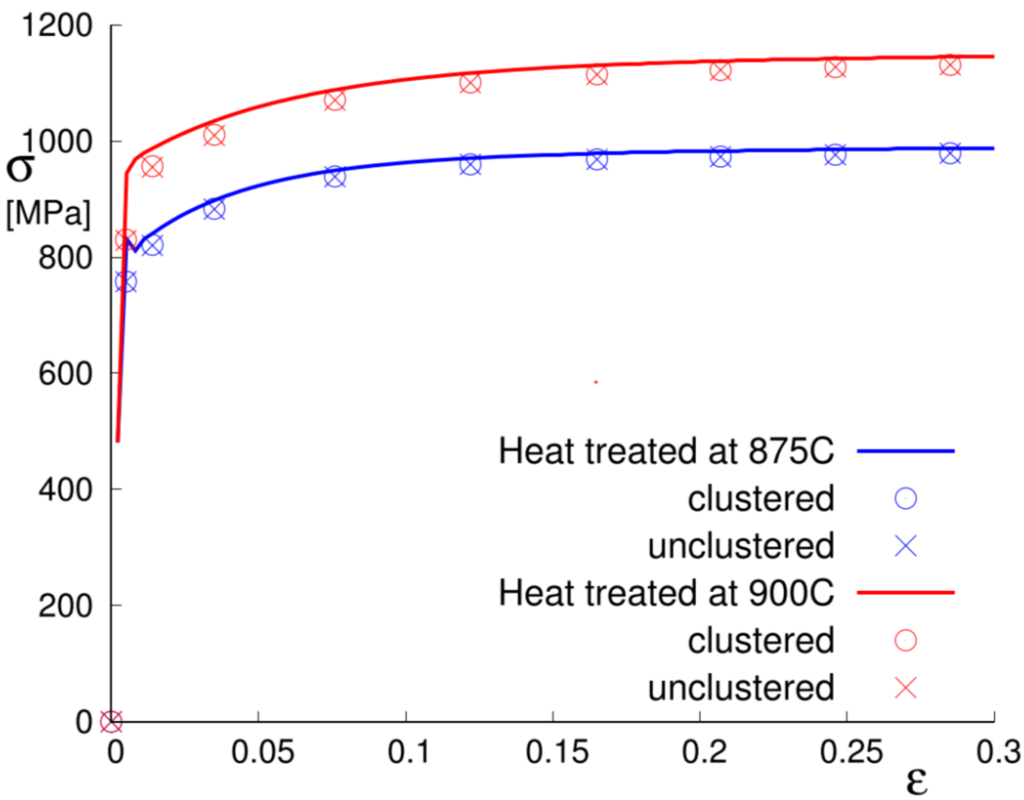

FIGURE 4. Macroscopic stress strain curves predicted using the mean field model (lines) and the FE model with clustered and unclustered microstructures (symbols).

Figure 4 demonstrates that both modelling approaches predict approximately the same macroscopic stress-strain curve whereas Table 3 shows local predictions in the ferrite phase. Whereas the mean field model provides only the per-phase averages of the stress and strain tensors, the FE model can be used to probe the heterogeneity inside each phase. According to Table 3, the plastic strain in ferrite (p^F) increases as a result of the heat treatment. The effect is stronger when considering the maximum local value in the clustered microstructure. Interestingly, the stress triaxiality in ferrite (ratio of the hydrostatic stress to the equivalent Von Mises stress) is much larger than the macroscopic value, which is 0.33 in an uniaxial tension test. The stress triaxiality, which dictates the rate of void growth after the onset of ductile damage, is strongly increased in the material heat treated at higher temperature (900°C). We note that, when compared to the FE predictions, the mean field model slightly underestimates the average value of p^F and it slightly overestimates the stress triaxiality in the ferrite.

TABLE 3. Model prediction of the strain localization in ferrite (ratio of the plastic equivalent strain to the macroscopic equivalent strain) as well as the stress triaxiality (trace of the local stress tensor divided by three times the local equivalent stress).

		Heat treated at 875°C		Heat treated at 900°C	
		$p^F / \varepsilon_{eq}^{macro}$	$\sigma_{ii} / (3\sigma_{eq})$	$p^F / \varepsilon_{eq}^{macro}$	$\sigma_{ii} / (3\sigma_{eq})$
Mean field	Avg.	1.23	0.53	1.27	0.62
FEM (clustered)	Avg.	1.27	0.46	1.31	0.51
	Max.	1.70	0.68	1.86	0.81
FEM (unclustered)	Avg.	1.27	0.45	1.31	0.49
	Max.	1.63	0.66	1.78	0.79

DISCUSSION

Mean field and finite element modelling has been used to study the effect of martensite carbon content on the strength and strain heterogeneity in a martensite-ferrite stainless steel. The strength prediction in fig. 4 is in good agreement with experimental trends (fig. 2a) showing an increase of the average strength of the material with an increase of martensite carbon content. Next, nanoindentation results indicated that while the strength of martensite increases with higher carbon content, ferrite strength does not increase by this mechanism. Thus, heat treatments produced microstructure with a large difference in strength between the two phases, which is suspected to promote strain heterogeneities in the microstructure, as already known from the literature [6].

Strain partitioning was studied with the finite element model shown in fig. 3. The results reported in Table 3 reveal strain localisation in the softer ferritic phase. On average, the strain in ferrite was found to increase as martensite strength increases, which agrees with other modelling results of dual phase microstructures [16, 17]. Next, the largest strain was observed in clustered ferrite for the microstructure heat treated at 900°C, here the strain was 90% larger than the macroscopic imposed strain. While damage was not considered in the model, large strain in ferrite could promote damage nucleation due to interface decohesion of coarse carbides and inclusions, as observed in the experiments.

Somewhat less expected was the observation of high triaxiality values in the ferrite phase, which for clustered microstructures was approximately 2.5 times larger than the normal triaxiality value for uniaxial tensile test (0.33). Considering the critical effect of stress triaxiality on damage evolution [22], these results could explain the observed reduction of the ductility in microstructures with large strength heterogeneity among phases.

Finally, FE results have shown that the distribution of ferrite inside the hard martensite scaffold had only a minor effect on both the strain partitioning and triaxiality values in the ferrite phase. Thus, the most important parameter is by far the strength difference between the two constituents of the microstructure.

CONCLUSION

A dual phase martensite-ferrite stainless steel was heat treated to alter the martensite carbon content, while keeping a constant phase ratio across the heat-treated microstructures. Three microstructures were selected for uniaxial tension and bending tests and finally the strain partitioning between the two phases was modelled. The main conclusions are as follow:

- Nanohardness measurements indicate that by increasing the martensite carbon content, the strength of martensite can be increased. This results to an increase of the mechanical (strength) contrast between the two phases.
- Macroscopic mechanical tests show a reduction of the ductility when the mechanical contrast between phases increases.
- Micromechanical modelling exhibit a clear strain partitioning in the ferrite phase, which increases in microstructures with larger strength contrast.
- Stress triaxiality 2.5 larger than the macroscopic value was observed in ferrite. This could lead to an increase of the nucleation and void growth rates and a reduction of ductility, as observed experimentally.
- Ferrite distribution (clustered vs unclustered) was found to have limited influence on strain partitioning.

All these observations lead to the general suggestion that in order to increase the ductility of dual phase microstructures, the strength difference between the constituents should be minimised. This is normally achieved in industrial practice with the tempering process, which causes the precipitation of a fine dispersion of carbides in martensite, thus decreasing the carbon content of the latter.

ACKNOWLEDGEMENTS

AMB's research at UCL is funded by APERAM. LD is mandated by the FRS-FNRS (Belgium).

REFERENCES

1. D. S. Codd "Automotive Mass Reduction with Martensitic Stainless Steel". *SAE International* (2011).
2. C. G. de Andrés, G. Caruana and L. F. Alvarez. *Materials Science and Engineering A* **241,** 211–215 (1998).
3. C. Liu, Y. Liu, D. Zhang, B. Ning and Z. Yan. *Steel Research Int.* **82,** 1362–1367 (2011).
4. C. Tasan. *Annual Review of Materials Research* **45,** 391–431 (2015).
5. J. Kang, Osokov, J. Embury and D. S. Wilkinson. *Scripta Materialia* **56,** 999–1002 (2007).
6. Q. Han, A. Asgari, P. D. Hodgson and N. Stanford. *Materials Science & Engineering A* **611,** 90–99 (2014).
7. H. Ghadbeigi, C. Pinna, and S. Celotto. *Materials Science & Engineering A* **588,** 420–431 (2013).
8. A.P. Pierman, O. Bouaziz, T. Pardoen, P. J. Jacques and L. Brassart. *Acta Materialia* **73,** 298–311 (2014).
9. M. D. Taylor. *Materials Science & Engineering A* **597,** 431–439 (2014).
10. A. W. Hudgins and D. K. Matlock. *Materials Science & Engineering A* **654,** 169–176 (2016).
11. A. Pineau, A. Benzerga and T. Pardoen. *Acta Materialia* **107,** 424–483 (2016).
12. F. M. Beremin. *Metallurgical Transactions A* **12A,** 723–731 (1981).
13. C. Landron, O. Bouaziz, E. Maire and J. Adrien. *Scripta Materialia* **63,** 973–976 (2010).
14. G. Avramovic-Cingara, C. A. R. Saleh, M. K. Jain and D. S. Wilkinson. *Metallurgical and Materials Transactions A* **40,** 3117–3127 (2009).
15. H. Kumar, C. L. Briant and W. A. Curtin. *Mechanics of Materials* **38,** 818 (2006).
16. T. W. J. de Geus, R. H. J. Peerlings and M. G. D. Geers. *International Journal of Solids and Structures* **67-68,** 326–339 (2015).
17. T. W. J. de Geus, F. Maresca, R. H. J. Peerlings and M. G. D. Geers. *Mechanics of Materials* **101,** 147–159 (2016).
18. L. Brassart, L. Delannay and I. Doghri. *International Journal of Solids and Structures* **47**, 716--729 (2010).
19. L. Delannay, P. J. Jacques, S. L. Kalidindi. *International Journal of Plasticity* **22**, 1879—1898 (2006).
20. G. Martin, S. K. Yerra, Y. Brechet, M. Véron, J. D. Mithieux, B. Chehab, P. J. Jacques and T. Pardoen. *Acta Materialia* **60**, 4646—4660 (2012).
21. A. Miotti Bettanini, L. Delannay, P. J. Jacques, T. Pardoen "Influence of carbon enrichment on the ductility of a martensite-ferrite stainless steel". *In preparation.*
22. T. Pardoen and J. W. Hutchinson. *Journal of the Mechanics and Physics of Solids* **48**, 2467—2512 (2000).